Solvent Effects in Active-Site Molecular Dynamics Simulations on the Binding of 8-Methyl-N5-Deazapterin and 8-Methylpterin to Dihydrofolate Reductase

PETER L. CUMMINS and JILL E. GREADY*

Department of Biochemistry, University of Sydney, NSW 2006, Australia

Received 17 March 1995; accepted 13 December 1995

ABSTRACT

Molecular dynamics (MD) simulation methods have been used to study the active site of the ternary complex formed between avian dihydrofolate reductase (DHFR), NADPH cofactor, and the inhibitor 8-methyl-N5-deazapterin in aqueous solution. Spherical shells of water molecules (initially at the bulk-solvent density) are used to solvate the active site and the surrounding protein surface. Two models for treating the effects of the neglected bulk solvent are then considered. The tethered water (TW) model is characterized by the use of harmonic restraining potentials to tether the water molecules to their initial (bulk solvent) positions; whereas, in the capped water (CW) model, water molecules are prevented from escaping from the solvent shell by the use of half-harmonic potentials, but otherwise their motions within the solvation shell are unrestrained. As measured by overall rms differences between coordinates, the distribution of solvent molecules in the active-site region, and the numbers of hydrogen bonds, the TW model compares favorably with the CW model but requires far fewer water molecules, i.e., relatively small solvent shells. The smaller shells of unrestrained water (CW model) gave rise to a distortion in the orientation of the side chain of the active-site residue Tyr-31, whereas no such distortion was apparent in the TW model or for the larger solvent shells in the CW model. A value for the force constant of 0.005 kcal/mol/Å^2 for the tethering potential [Solmajer and Mehler, *Int. J. Quant. Chem.*, **44**, 291 (1992)] gave satisfactory results for DHFR, although we found that distance-dependent

* Author to whom all correspondence should be addressed at: Division of Biochemistry and Molecular Biology, John Curtin School of Medical Research, Australian National University, P.O. Box 334, Canberra ACT 2601, Australia.

Journal of Computational Chemistry, Vol. 17, No. 14, 1598–1611 (1996)
© 1996 by John Wiley & Sons, Inc.
CCC 0192-8651 / 96 / 141598-11

dielectric functions were unable to reproduce accurately the effects of the explicit water models. The free-energy change for the mutation of 8-methyl-N5-deazapterin to 8-methylpterin was computed using both nonsolvated and solvated models. The solvated models gave free energy differences about 1 kcal/mol lower than for nonsolvated models, but the differences between solvated models was much less than 1 kcal/mol. Overall, the calculated differences in thermodynamic stability of the deazapterin and pterin complexes are in fair agreement with experiment, i.e., a small binding differential is predicted. © 1996 by John Wiley & Sons, Inc.

Introduction

As proteins perform their biological functions in aqueous solution, the modeling of solvent effects in molecular simulations is often critical to the reliable prediction or interpretation of experimental results. However, the inclusion of sufficient numbers of water molecules in a molecular dynamics (MD) simulation requires an excessive amount of computer time to solvate effectively all but the smallest proteins. Simulations must be performed on systems of finite size and the effect of the neglected surroundings approximated by the introduction of external potentials. Newton's equation of motion for a particle in the system then reads:

$$m_i \mathbf{a}_i = \sum_{j \neq i} \mathbf{F}_{ij} + \mathbf{F}_{\text{ext}} \qquad (1)$$

where $\mathbf{F}_{ij}$ is the force acting on atom i due to interactions between other particles in the system and $\mathbf{F}_{\text{ext}}$ is the force on atom i exerted by the (implicit) surroundings. In bulk liquid simulations the external force is usually approximated by the application of periodic boundary conditions and is, therefore, of the type $\mathbf{F}_{ij}$, i.e., due to interactions with nearest-neighbor images. Due to the high computational cost of explicitly including bulk-solvent effects by the imposition of periodic boundary conditions in macromolecular dynamics simulations, several approximate methods have been proposed for treating the effects of solvent on protein structure and dynamics. In the simplest treatments of solvent effects in protein simulations, the contributions to $\mathbf{F}_{ij}$ from coulomb interactions are scaled down to account for electrostatic screening of charged groups by the bulk solvent. Although a number of such dielectric functions have been proposed for protein simulations, it appears clear that a more complete description of protein–solvent interactions is required.[1,2] Models based on electrostatic screening alone neglect such phenomena as hydrophobic hydration and the frictional forces due to van der Waals contacts between water molecules and the protein. Continuum approaches may be useful in modeling electrostatic, hydrophobic hydration and van der Waals forces on solvated systems,[3-5] but these methods have yet to be implemented as a consistent whole within a molecular dynamics simulation scheme. Moreover, specific hydrogen-bond (H-bond) interactions are likely to present difficulties for these models. MD simulations of proteins in explicit water have shown that protein–protein side chain H-bonds may be replaced by protein–solvent H-bonds.[6] Changes in other properties such as increases in the solvent-accessible surface area of proteins have also been reported.[7-10]

In the application of computer simulation methods in areas such as drug design, one is primarily interested in the region of the protein which binds a substrate or inhibitor, i.e., the active-site region. The details of the environment, i.e., the rest of the protein and solvent in which the active site is embedded, are of concern only to the degree they influence properties of the active site. Consequently, if the extended environment can be modeled adequately, the molecular dynamics simulation may be confined to the active site thus rendering simulation studies on ligand binding computationally feasible for any protein of known crystal structure.[11,12] In this work we have examined how different ways of including solvent influence the structural details of the active-site region and also the computed free-energy change[13,14] for the mutation between similar ligands of dihydrofolate reductase (DHFR), an important drug target for the treatment of infectious diseases and cancer.[15]

The ligands we have chosen for this study are 8-methylpterin, a new substrate of DHFR,[16,17] and

the new inhibitor 8-methyl-N5-deazapterin,[18] both protonated at N3 as shown in Figure 1. These ligands are assumed to be H-bonded to the enzyme via a conserved Asp (bacterial) or Glu (vertebrate) side chain in the active site.[19-21] Following the approach of Solmajer and Mehler,[22] we have attempted to model the effects of bulk solvent by the introduction of dynamically restrained water molecules in the MD simulations. Solmajer and Mehler have proposed to model the solvent effects on protein dynamics empirically by the introduction of a distance-dependent dielectric function and a limited number of dynamically restrained water molecules at the protein surface. The relative simplicity of the restrained molecular dynamics approach and its ease of implementation within MD simulations, as compared with the stochastic-equation approaches,[11,12] lead us to investigate the use of such models in the active-site dynamics of DHFR. In the absence of explicit solvent (i.e., other than crystallographic waters) we have also performed MD simulations using two distance-dependent dielectric functions.[1,23] The dynamically restrained and dielectric-solvent models are compared with the results obtained from simulations in which unrestrained water molecules have been included as larger solvation shells (up to a 34 Å radius) centered on the active site. Root-mean-square (rms) differences in atomic coordinates, solvent distributions, H-bonding interactions, and variations in ligand-binding free energies for mutation between the two cations (Fig. 1) are compared for the different solvation models. The free energy of binding, in particular, is often a sensitive probe of changes in environment, and a quantity used in the design of biologically active molecules.[20,21] The computed free-energy changes are compared with the corresponding experimental difference for the two cations.

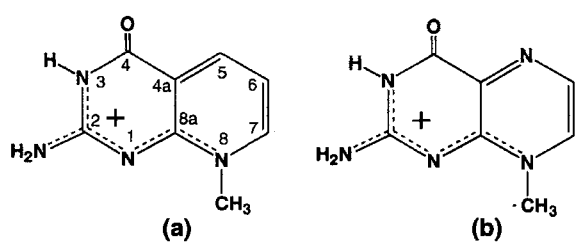

FIGURE 1. Structures of the N3 protonated (a) 8-methyl-N5-deazapterin and (b) 8-methylpterin cations showing the extended-guanidinium resonance.

Methods

MODEL FOR THE ENZYME ACTIVE SITE IN SOLVENT

The functional form for the configurational energy of the system is given by:

$$V = V_{\text{bad}} + V_{\text{ele}} + V_{\text{vdW}} + V_{\text{ext}} \quad (2)$$

where V_{bad} includes all bond, angle, and dihedral terms; V_{ele} is the electrostatic term arising from nonbonded interactions between atomic charges, and V_{vdW} is the nonbonded van der Waals (vdW) interaction term. V_{ext} is an external potential energy used to restrain the dynamics of solvent molecules. The individual terms are given by[24,25]:

$$V_{\text{bad}} = \sum_{\text{bonds}} K_b(R - R_0)^2 + \sum_{\text{angles}} K_a(\theta - \theta_0)^2 + \sum_{\text{dihedrals}} \left[\frac{K_d}{2}[1 - \cos(n\Phi - \gamma)] + V_{14}\right] \quad (3)$$

$$V_{\text{ele}} = \sum_{i<j} \frac{q_i q_j}{\varepsilon R_{ij}} \quad (4)$$

$$V_{\text{vdW}} = \sum_{i<j} \left[\frac{A_{ij}}{R_{ij}^{12}} - \frac{B_{ij}}{R_{ij}^{6}}\right] \quad (5)$$

The V_{14} interactions (i.e., the interactions between first and last atoms of a given proper dihedral angle) in eq. (3) are given by electrostatic plus vdW (6–12 Lennard–Jones) terms as in eqs. (4) and (5) scaled by a factor of one half.[25] The force-field parameters for the NADPH cofactor are given in an earlier work.[26] The ligand parameters were derived from AM1[27] calculations as described previously.[28] The TIP3P model[29] was used for water molecules, and the force-field parameters of Weiner et al.[24,25] were used for the protein. For protein residues within 8 Å of the ligand, the all-atom force field[25] was used, whereas for the remainder of the protein we have used the computationally more efficient united-atom model[24] in which hydrogens attached to carbon are not explicitly defined. Although the force fields of Weiner et al.[24,25] use a 10–12 potential function for the protein–protein H-bonds, we have omitted explicit vdW interaction terms for H-bonded pairs to obtain a consistent and complete description of all possible H-bonding,[30,31] i.e., for both protein–protein and protein–solvent. The H-bonded pairs for protein–protein and protein–solvent interactions were de-

fined by neglecting the vdW terms for electronegative atoms (X = N, O, or S) and donor H atoms, subject to the geometrical requirement that the distance between proton acceptor (X) and proton was less than 2.5 Å and the corresponding $X \cdots H\text{–}X'$ angle was greater than 130°. The effect of introducing this discontinuity in the vdW terms was found to be negligible due to the low values of the energies involved and the R^{-6} dependence.

The effect of electrostatic screening in simulations carried out without explicit solvent (other than crystallographic water molecules) has been treated using distance-dependent dielectric functions, ε in eq. (4). The function proposed by Kim truncates the electrostatic interactions smoothly,[23] i.e., removes the discontinuity in the electrostatic energy at the cutoff:

$$\begin{aligned} \varepsilon &= \left[1 - (R_c/R_{ij})^2\right]^{-3} && R_{ij} < R_c \\ &= 0 && R_{ij} > R_c \end{aligned} \qquad (6)$$

where R_c is the cutoff distance for the neglect of interactions, while the Solmajer and Mehler function[1] approaches the dielectric constant of water at large interatomic distances:

$$\varepsilon = A + B/\left[1 + k\exp(-\lambda B R_{ij})\right] \qquad (7)$$

where $B = \varepsilon_\infty - A$, $\varepsilon_\infty = 78.4$ is the dielectric constant of water and $A = -8.55$, $k = 7.78$, and $\lambda = 0.00363$. In the simulations with added solvent, i.e., solvent other than the crystallographically determined water, a constant dielectric of $\varepsilon = 1$ was used.

The introduction of the external potential, V_{ext}, in eq. (1) is designed to mimic the effect of the surrounding (implicit) bulk solvent on the system by restricting the movement of any explicit water molecules.[22] Thus, V_{ext} arises from the force exerted on the explicit atoms by the implicit surrounding bulk solvent. This restraining potential has the simple harmonic form:

$$V_{ext} = \sum_i \frac{k_i}{2}(R_{ix})^2 \qquad (8)$$

where R_{ix} is the distance from atom i of a water molecule to a fixed reference point x, and k_i is the empirically determined force constant. We consider two models for the inclusion of bulk–solvent effects in the MD simulations, each based on the use of the external potential, V_{ext}, given by eq. (8) with the same force constant $k = k_i$ assumed for all atoms. In the capped water (CW) model, R_{ix} is the distance of a water molecule's atom i from the ligand center minus the radius of the spherical solvation shell (R_w). Thus, the CW model simply prevents water from escaping the dynamics region, but otherwise the water molecule dynamics are not directly affected by an external potential. This model has been widely used in active-site simulations,[14] usually with a force constant of k = 0.6 kcal/mol/Å^2.[20,21,32] If R_w could be made sufficiently large, the bulk solvent would effectively be simulated. In the "tethered" water (TW) model, R_{ix} is the distance of the water oxygen from its initial bulk solvent or crystallographic positions. Taking account of theoretical (MD simulation) studies[8] that suggest water dipoles align tangentially to protein surfaces, we apply V_{ext} only to the oxygen atoms, allowing water molecules to attain their preferred orientations without artificially hindering their librational degrees of freedom.

Solmajer and Mehler have modeled the effects of solvent on the dynamics of bovine pancreatic trypsin inhibitor (BPTI) using a TW model in conjunction with a dielectric function [eq. (7)] to model electrostatic screening.[22] The force constant for the external potential is chosen to produce a trajectory as similar as possible to that obtained in a "BOX" simulation in which the bulk solvent is explicitly modeled with the imposition of periodic boundary conditions. For simulations involving only crystallographic water, values of k = 2.5 and k = 25 kcal/mol/Å^2 were tested, with the former giving the trajectory closer to the BOX simulation.[22] However, including the first hydration shell (of 3-Å thickness) in the simulation, a value of k = 0.005 kcal/mol/Å^2 was found to give better results.[22] We have tested values of k = 25, 2.5, and 0.005 in the present work on the active-site MD of DHFR.

The starting coordinates for the DHFR molecule, NADPH cofactor, and 199 crystallographic water molecules were taken from the clDHFR.NADP$^+$. biopterin X-ray structure.[33] The biopterin moiety is readily replaced by 8-methyl-N5-deazapterin since both appear to bind in the same orientation.[20,21] All ionizable amino acid residues were assumed to be in their charged states and were not neutralized by counterions in the simulations. In the active-site approach, a molecular dynamics zone is defined by including all residues (amino acid plus water) within a certain radius of the active site, thus partitioning the system into "nondynamic" atoms whose positions are frozen at the initial X-ray coordinate values and "dynamic" atoms which are the only ones allowed to move during the various

stages of the calculations. As in a previous MD study on DHFR-binding ligands,[21] the active-site dynamics zone was confined to a radius of ca. 16 Å from the ligand. Thus, we have included in the protein dynamics all DHFR amino acid residues and crystallographic waters within this radius. The 16-Å radius includes 46 crystallographic water molecules in the dynamics region, and provides sufficient room for only a few water molecules from the bulk solvent. We have used radii (R_w) up to 34 Å for the inclusion of bulk water in the dynamics, where the solvation radius R_w is defined as the radius from the center of the ligand to the edge of the solvation shell. The initial coordinates of the added solvent molecules in the CW and TW models were obtained by immersing the DHFR complex in a solvent box constructed from Jorgensen's Monte Carlo simulations of bulk solvent using the TIP3P-model for water molecules.[29] Water molecules beyond the radius R_w were deleted along with those having an interatomic distance with the protein of less than 3 Å. The details of the various solvated-protein models are summarized in Table I.

ANALYSIS

Solmajer and Mehler used the rms deviations from both X-ray and the bulk solvent simulations as the criteria for choosing the force constant k and assessing the models.[22] In addition to overall rms deviations, we computed rms deviations with respect to the secondary structure elements given in Table II. The solvent numbers are given for the first hydration shell in the initially solvated complexes as an indication of the overall solvent accessibility of each element. R_{min} gives the minimum distance between the ligand and the secondary structure element. To analyze further the solvent effect on protein structure the complex was divided into three spherical shells of 6-Å thickness with the origin at the ligand center. The residues within each shell in the CW (R_w = 34 Å) model were then determined and the rms deviations in atomic positions from the corresponding residues in the other structures computed.

We also compare the solvent distributions around the active-site region, and other structural details such as the protein–protein and protein–solvent H-bonding. To analyze the solvent distributions in the active site for the different solvent models, we found it convenient to define the solvent density as a function of distance from the DHFR active site as:

$$\rho(r) = r^{-3}n(0, r) \tag{9}$$

where $n(0, r)$ is the number of water molecules contained within a radius $r = 0$ and r from the C8a atom of the 8-methyl-N5-deazapterin ligand, and thus $n(0, R_w) = N_w$ is the total number of water molecules within the shell.

TABLE I.
Solvated-Protein Models.

Model[a]	R_w[b]	N_w[c]	Description
CW	16	46	Crystallographic water only (capped water)
CW	22	392	Solvent shell (capped water)
CW	26	1033	Solvent shell (capped water)
CW	30	2135	Solvent shell (capped water)
CW	34	3763	Solvent shell (capped water)
TW	16	46	Crystallographic water only (tethered water)
TW	19	155	Solvent shell (tethered water)
TW	22	392	Solvent shell (tethered water)
TW	26	1033	Solvent shell (tethered water)

[a] CW = capped water, TW = tethered water (see text). k = 0.6 kcal/mol/Å^2 for CW models or k = 25, 2.5, and 0.005 kcal/mol/Å^2 for TW models (see text).
[b] Radius (Å) of solvation sphere.
[c] Numbers of dynamical water molecules within solvation sphere.

FREE-ENERGY CALCULATIONS

Free-energy differences for the binding of the two ligands (Figure 1) have been computed using thermodynamic integration methods.[13] The potential energy function, $V(\lambda)$, for the ligand–protein interactions is expressed in the form:

$$V(\lambda) = \lambda V(1) + (1 - \lambda)V(0) \tag{10}$$

where at $\lambda = 1$ the bound 8-methyl-N5-deazapterin state [$V(1)$] is described, and at $\lambda = 0$ the bound 8-methylpterin state [$V(0)$] is described. The thermodynamic integration calculations were performed using the continuous coupling (slow growth) approach, where λ varies continuously and linearly between the two states with the MD simulation time step. The free-energy difference, ΔA, between states defined by $V(1)$ and $V(0)$ is then easily computed from the numerical integration formula:[28]

$$\Delta A = N^{-1} \sum_{i=1}^{N} [V(1) - V(0)]_i \tag{11}$$

TABLE II.
Secondary Structural Elements of clDHFR.

Secondary structure	Sequence numbers	Sequence numbers < 16Å [a]	Solvent number[b]	R_{min} (Å)[c]
βA	4–10	4–10	1.7	5.3
loop (L1)	11–27	11–27	9.0	6.8
αB	28–40	28–40	11.3	4.7
loop (L2)	41–47	—	12.6	—
βB	48–54	48–54	2.1	10.5
αC	55–60	55–60	7.2	8.7
loop (L3)	61–70	61, 62, 64–70	14.5	10.9
βC	71–76	71–75	1.2	14.1
loop (L4)	77–86	—	10.8	—
βD	87–90	—	7.8	—
αE	92–101	93	4.6	14.6
αE′	105–109	—	9.0	—
βE	111–116	111–116	3.2	10.6
αF	118–127	118–125	5.3	9.8
βF	131–139	131–139	5.5	8.4
loop (L5)	140–156	140, 142–149, 151	11.2	11.5
βG	157–172	164–166, 170, 172, 173	10.4	14.5
βH	176–183	175–182	8.4	12.0

[a] Residues included in the active-site dynamics zone.
[b] Average number of solvent molecules (per residue) within 3.5 Å of the protein based on the initially solvated CW (R_w = 34 Å) complex.
[c] Minimum atom-to-atom distance from the secondary structure element to the ligand.

where N is the number of integration time steps and $[V(1) - V(0)]_i$ is the difference evaluated using the configuration obtained at the ith time step in the MD simulation.

SIMULATION CONDITIONS

The MD equations were integrated using the constant temperature procedure of Berendsen et al.[34] with the SHAKE algorithm[35] to constrain all bond lengths to their specified equilibrium (R_0) values. The temperature was set at 300 K with velocity scaling:

$$s = \left[1 - \frac{\Delta t}{\tau}\left(\frac{T_0}{T} - 1\right)\right]^{1/2} \qquad (12)$$

at each time step (Δt = 0.002 ps). The relaxation time, τ, was set to a value (ca. 0.02 ps) similar to that used by Solmajer and Mehler.[22] Appropriate choice of the frequency for updating the nonbonded interaction lists is dependent on the cutoff and other conditions such as the time step, temperature, and relaxation time. In the present simulations we have used a 9-Å residue-based cutoff for the nonbonded interactions, with the minimum distance between residues as the cutoff distance. Under these conditions we have found that the generally recommended frequencies are too conservative. Based on results obtained from our previous calculations on solvated DHFR-binding ligands,[28] the nonbonded interaction lists (including H-bonds) were updated every 100 time steps (0.2 ps). All calculations were performed using locally developed software.[28]

The systems including protein, NADPH, ligand, and water were initially energy minimized using conjugate gradients until the rms gradients were below 3 kcal/mol/Å. For models with solvent-shell water (R_w > 16 Å), the initial energy minimization was performed for the solvent only, keeping the ternary complex fixed at the X-ray structure, followed by the simultaneous energy minimization of the complex and water. After the energy minimizations, the solvent was equilibrated (keeping the ternary complex coordinates fixed) for 4 ps of MD. The length of time a trajectory was allowed to run before sampling configu-

rations for analysis was determined by monitoring the overall rms deviations of the DHFR coordinates from the initial X-ray values. Once a trajectory was considered to have converged, sampling took place over the next 40 ps. Thermodynamic integration (TI) calculations were then carried out over simulation times of 80 ps in forward and reverse directions. Additional TI calculations (80 ps) were performed without truncation of the ligand–protein and ligand–solvent interactions (all other interactions subject to the 9-Å cutoff), after a 10-ps equilibration with the extended cutoff.

Results and Discussion

ROOT-MEAN-SQUARE DIFFERENCES

The root-mean-square (rms) deviations of the DHFR coordinates from the original X-ray values for the CW model trajectories are plotted as a function of simulation time in Figure 2. Analogous trajectory plots for the TW models are shown in Figure 3. In both the CW and TW models the trajectories generally become more damped in the start-up phase of the simulation as the size of the solvation sphere is increased and, hence, equilibration times tend to be longer for simulations with added solvent. As expected,[22] trajectories with highly restrained crystallographic water molecules (TW models with k = 25 and 2.5 kcal/mol/Å^2) deviate much less from the initial X-ray structure and equilibration is effectively complete within 100 ps. Convergence in the remaining TW and CW model trajectories appears satisfactory after ca. 100 ps. The rms deviations of the averaged DHFR coordinates from both the initial X-ray and average CW model (R_w = 34 Å) values for all of the CW and TW solvent models are given in Table III. All MD coordinates have been averaged over the last 40 ps of the trajectory times indicated in Table III. The averaged structures were not energy minimized for the calculation of rms deviations.

Constraining sections of the protein (in the present case ca. 30% of residues) in the dynamics reduces the conformational flexibility of the protein. Consequently, compared with simulations on the unconstrained protein in water,[26] the overall rms deviations are much reduced in active-site dynamics. For the CW model, neither the C_α backbone nor all-atom rms deviations from the X-ray structure appear to follow any trend with increase in size of the solvent shell. However, rms deviations from CW (R_w = 34 Å) steadily decrease, indicating that successive structures tend to become more alike with increasing R_w. Restraining the crystallographic waters with a relatively large force constant (TW model with k = 25 or 2.5) results in coordinate values which are closer to the initial X-ray (rmsd < 0.9 Å), but further from those obtained from the CW model (rmsd > 1.0 Å). However, the TW models with k = 0.005 and R_w > 19 Å give rise to relatively smaller rms deviations from the CW (R_w = 34 Å) model. Thus, on the basis of the overall rms deviations, weakly restrained shells of solvent appear to be the more characteristic of the approximate bulk-solvent simulation (R_w = 34 Å) results.

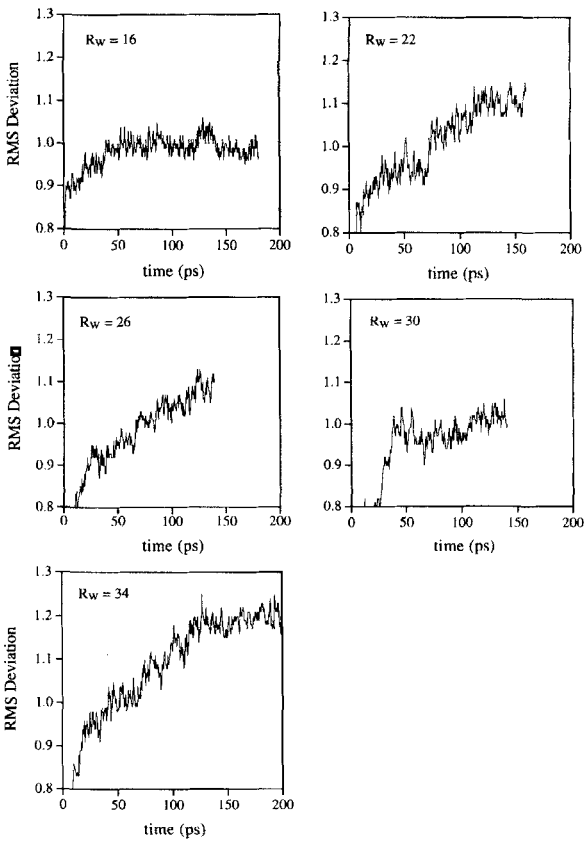

FIGURE 2. The rms deviations (Å) from X-ray coordinates of the DHFR molecule as a function of simulation time for the capped water (CW) model. R_w is the radius (Å) of the solvation sphere.

The C_α rms deviations for the secondary structure elements (Table II) are given in Table IV. The rms deviations are found to be generally smaller for β sheets and α helices than for loops (L1, L3, and L5), as might be predicted. For a given model, L1 generally shows by far the largest deviation among the secondary structures. The only excep-

TABLE III.

rms Deviations (Å) of Mean Simulation DHFR Coordinates from X-Ray and Mean Simulation CW, R_w = 34 Å Model DHFR Coordinates.

Model[a]	$\varepsilon(R)$	R_w[b]	N_w[c]	time[d]	rms from X-ray[e]		rms from CW[f]	
					C_α	All atom	C_α	All atom
CW	1	16	46	140	0.42	0.95	0.67	0.99
CW	1	22	392	160	0.63	1.04	0.65	0.91
CW	1	26	1033	140	0.42	1.00	0.51	0.76
CW	1	30	2135	140	0.46	0.95	0.49	0.72
CW	1	34	3763	140	0.65	1.12	0.00	0.00
TW (k = 25)	1	16	46	120	0.36	0.84	0.64	1.08
TW (k = 2.5)	1	16	46	140	0.37	0.83	0.57	1.02
TW (k = 0.005)	1	16	46	140	0.45	0.99	0.58	0.93
TW (k = 0.005)	eq. (6)	16	46	140	0.52	0.93	0.81	1.18
TW (k = 0.005)	eq. (7)	16	46	140	0.73	1.10	0.80	1.36
TW (k = 0.005)	1	19	155	160	0.52	1.02	0.69	0.99
TW (k = 0.005)	1	22	392	180	0.54	1.09	0.48	0.80
TW (k = 0.005)	1	26	1033	140	0.53	0.98	0.30	0.70

[a] CW = capped water, TW = tethered water (see text). k = force constant for restraining potential (kcal/mol/Å^2).
[b] Radius (Å) of solvation sphere.
[c] Numbers of dynamical water molecules within solvation sphere.
[d] Times of trajectories in ps.
[e] rms deviations in MD coordinates of DHFR atoms. Coordinates averaged over last 40 ps of trajectories.
[f] CW (R_w = 34 Å) model. Coordinates averaged over last 40 ps of trajectories.

tion is for TW (R_w = 26 Å) in which L5 gives the largest deviation, although in this case the overall deviations are much smaller than for the other models. The smaller rms deviations observed for β sheets (max. 0.46) tend to coincide with relatively small solvent numbers (βA, βB, and βC in Table II), compared with the results for α helices (αB and αC) where rms deviations are larger (max. 1.03) as are the solvent numbers. As for many of the α helices, the loops tend to be highly exposed

TABLE IV.

C_α rms Deviations (Å) of Mean Simulation DHFR Coordinates From Mean Simulation CW, R_w = 34 Å Model DHFR Coordinates for Secondary Structure Elements in Table II.

Model[a]	R_w[b]	βA	L1	αB	βB	αC	L3	βC	βE	αF	βF	L5	βG	βH
CW	16	0.25	1.27	0.62	0.27	0.29	0.94	0.20	0.20	0.34	0.19	0.78	0.15	0.18
CW	22	0.27	1.24	0.61	0.27	0.24	1.19	0.18	0.17	0.19	0.18	0.32	0.32	0.26
CW	26	0.17	1.06	0.56	0.21	0.25	0.37	0.10	0.10	0.25	0.16	0.52	0.16	0.13
CW	30	0.23	1.08	0.29	0.26	0.32	0.29	0.07	0.11	0.26	0.17	0.50	0.12	0.10
TW (k = 25)	16	0.30	1.23	0.67	0.26	0.28	0.60	0.16	0.18	0.30	0.16	0.83	0.19	0.25
TW (k = 2.5)	16	0.23	1.05	0.66	0.23	0.26	0.58	0.12	0.14	0.30	0.21	0.79	0.24	0.24
TW (k = 0.005)	16	0.27	1.02	0.66	0.24	0.38	0.75	0.19	0.21	0.30	0.20	0.74	0.13	0.20
TW (k = 0.005)	16[c]	0.23	1.75	0.60	0.26	0.61	0.91	0.19	0.18	0.47	0.16	0.54	0.06	0.23
TW (k = 0.005)	16[d]	0.32	1.50	0.95	0.29	0.51	0.66	0.36	0.27	0.65	0.25	0.87	0.10	0.46
TW (k = 0.005)	19	0.28	1.28	0.76	0.21	1.03	0.79	0.16	0.13	0.21	0.33	0.61	0.17	0.23
TW (k = 0.005)	22	0.28	0.97	0.36	0.22	0.19	0.53	0.16	0.16	0.16	0.19	0.60	0.09	0.17
TW (k = 0.005)	26	0.24	0.45	0.19	0.12	0.10	0.19	0.08	0.11	0.13	0.14	0.67	0.27	0.13

[a] CW = capped water, TW = tethered water (see text). k = force constant for restraining potential (kcal/mol/Å^2).
[b] Radius (Å) of solvation sphere.
[c] Eq. (6).
[d] Eq. (7).

to solvent. Note that βG and βH, although highly exposed to solvent, show quite smaller deviations due to the constrained residues in the sequence. There is a marked reduction in the rms deviations for αB and L3 as the solvent shell is increased (CW) or tethering potentials are used (TW). However, compared with the TW model, the CW model gives a much smaller reduction in the rms deviations for L1 as the solvent radius is increased. The final loop in the sequence (L5) actually gives slightly worse rms deviations as solvent radius is increased and tethering potentials are used. Thus, the effect of solvent on the loop segments of the protein are much less predictable due to their greater conformational flexibility, whereas more systematic reductions in rms deviations are obtained for the α helices.

The all-atom rms deviations for spherical shells radiating from the active site center, as described in the Methods section are given in Table IV. The rms deviations in the first protein shell (0–6 Å) are always less than in the second shell (6–12 Å). This implies that the structural similarities among different models are greatest at the inner core of the dynamics zone. In fact, the rms deviations for R_w = 16 are less than for many of the solvated models in this region. Note that the third shell (> 12 Å) incorporates the boundary (at 16 Å) of the dynamics zone and, consequently, smaller rms deviations than in the second shell are often observed due to the damping influence of the constrained parts of the protein on nearby dynamical residues.

TABLE V.

All-Atom rms Deviations (Å) of Mean Simulation DHFR Coordinates From Mean Simulation (CW, R_w = 34 Å model) DHFR Coordinates for Shells of Protein.

Model[a]	R_w [b]	Shell(Å)		
		0–6	6–12	> 12
CW	16	0.70	1.02	1.03
CW	22	0.89	0.96	0.85
CW	26	0.69	0.83	0.70
CW	30	0.59	0.80	0.64
TW (k = 25)	16	0.73	1.19	1.04
TW (k = 2.5)	16	0.68	1.08	1.04
TW (k = 0.005)	16	0.52	0.93	1.02
TW (k = 0.005)[c]	16	1.29	1.30	0.99
TW (k = 0.005)[d]	16	1.00	1.52	1.24
TW (k = 0.005)	19	0.92	1.01	0.99
TW (k = 0.005)	22	0.65	0.87	0.77
TW (k = 0.005)	26	0.53	0.62	0.84

[a] CW = capped water, TW = tethered water (see text). k = force constant for restraining potential (kcal/mol/Å^2).
[b] Radius (Å) of solvation sphere.
[c] Eq. (6).
[d] Eq. (7).

HYDROGEN BONDING AND ELECTROSTATIC SCREENING

The results of an analysis of the proton–acceptor interactions using the 2.5-Å distance and 130° angle criteria (see Methods) for defining H-bonds are given in Table VI. The numbers of protein–protein H-bonds are reduced in the presence of explicit solvent, whereas the Solmajer–Mehler (SM) function [eq. (7)] grossly overestimates this reduction. Using the SM function, an average of 82 protein–protein H-bonds for the simulation are obtained, compared with values ranging from about 113 to 133 for all other simulations. Application of eq. (6) produces no reduction in the number of protein–protein H-bonds. Thus, neither dielectric function appears to model adequately the effects of explicit solvent on the protein–protein H-bonding. The CW and TW models yield similar numbers of H-bonds; approximately one third of protein residues are involved in H-bonding with other protein residues. The proportions involved in H-bonding with solvent are much larger (two thirds at solvent saturation) than for protein–protein interactions.

In simulations in which solvent shells have been included (i.e., for R_w > 16 Å) the effects of electrostatic screening should at least be partially accounted for. In principle, it may be expected that these effects should also be accounted for when the dielectric function is applied in simulations without additional solvent (R_w = 16 Å). However, this does not appear to be the case, as it is apparent that both eqs. (6) and (7) yield averaged structures that are more unlike the CW (R_w = 34 Å) model than any of the other solvated model results, including those containing only crystallographic water (Table III). Consequently, it does not seem useful to attempt to combine a screening function with a solvent shell. The application of eq. (6) yields smaller overall deviations from the X-ray structure and eq. (7) produces the largest distortions in the backbone coordinates of all the simulations. The loss of H-bonding (Table VI) and larger deviations in the backbone coordinates (Table III)

TABLE VI.
Numbers of Hydrogen Bonds Obtained From Solvated-Protein Models.

Model[a]	$\varepsilon(R)$	R_w[b]	N_w[c]	Number of H-bonds[d]	
				Protein–protein[e]	Protein–solvent[e]
CW	1	16	46	130 (0.36)	72 (0.26)
CW	1	22	392	120 (0.36)	213 (0.52)
CW	1	26	1033	121 (0.36)	301 (0.64)
CW	1	30	2135	122 (0.35)	345 (0.67)
CW	1	34	3763	113 (0.34)	339 (0.66)
TW (k = 0.005)	1	16	46	133 (0.37)	60 (0.22)
TW (k = 0.005)	Eq. (6)	16	46	132 (0.38)	70 (0.25)
TW (k = 0.005)	Eq. (7)	16	46	82 (0.29)	19 (0.09)
TW (k = 0.005)	1	22	392	122 (0.36)	217 (0.53)
TW (k = 0.005)	1	26	1033	125 (0.37)	303 (0.62)

[a] CW = capped water, TW = tethered water (see text). k = force constant for restraining potential (kcal/mol/Å^2).
[b] Radius (Å) of solvation sphere.
[c] Numbers of dynamical water molecules within solvation sphere.
[d] Averages obtained over the 4-ps period of MD by sampling configurations at intervals of 0.1 ps.
[e] Results in parentheses are the fractions of protein residues involved in H-bonding.

obtained using the SM function is due to the much larger reduction in the electrostatic binding energy, as compared with the use of eq. (6). It should be noted here that the potential model used to describe H-bonding relies entirely on the electrostatics for binding as it neglects an explicit H-bonding energy term (see Methods). Other force-field models that include an explicit H-bond vdW term may preserve H-bonding despite the loss of electrostatic binding energy.[1,22]

The distorting effects of strong coulombic interactions on protein conformation in vacuum simulations may be damped by the use of electrostatic screening functions,[22] thereby reducing overall rms deviations from the starting X-ray structure in simulations on the unconstrained protein. However, the smaller more localized conformational changes that are likely to be important in active-site dynamics may not be well described. Although they produce smaller overall rms deviations relative to unscreened potentials, dielectric functions can yield a wide range of rms deviations and do not always give structures close to that obtained for the protein in explicit water.[36,37] A recent review by Smith and van Gunsteren provides a good discussion of the difficulties encountered when using dielectric functions in protein simulations.[38]

SOLVENT IN THE ACTIVE-SITE

Figure 4 shows a plot of the solvent density $\rho(r)$ for the CW models. All CW models yield a density profile which is larger than that determined from the initial configuration of solvent molecules obtained from bulk-water simulation.[29] However, the solvent has a tendency to contract away from the active site becoming more like the bulk density profile as the solvent shell is increased from R_w = 22 to 30 or 34 Å. Note that the solvent-density profiles for R_w = 30 and R_w = 34 Å are quite similar. Figure 5 shows the solvent densities for the TW model and CW (R_w = 34 Å) model for comparison. The solvent-density profiles obtained for the TW models with R_w < 26 Å are similar to those obtained with the CW (R_w = 30 and 34 Å) models.

Figures 6 and 7 show stereoplots of the active-sites from the CW (R_w = 22 Å) and TW (R_w = 22 Å) model simulations, respectively. In each case the pocket which would bind the methylene-*p*-aminobenzoyl-L-glutamate (pABA-Glu) group at the C6 position of the natural substrate (folate) is occupied by a number of water molecules. However, in the CW model the side chain of Tyr-31 has an orientation very different from that seen in the TW model. The orientation in the CW model allows additional solvent molecules into the active site. This accounts for the peak in the solvent density at approximately 6.5 Å in Figure 4, an artifact not seen in the most heavily solvated CW structures (R_w > 26 Å) or in any of the TW models. Figure 8 shows that the orientation of the Tyr 31 side chain in the CW (R_w = 34 Å) model is indeed similar to the one shown in Figure 7 for the

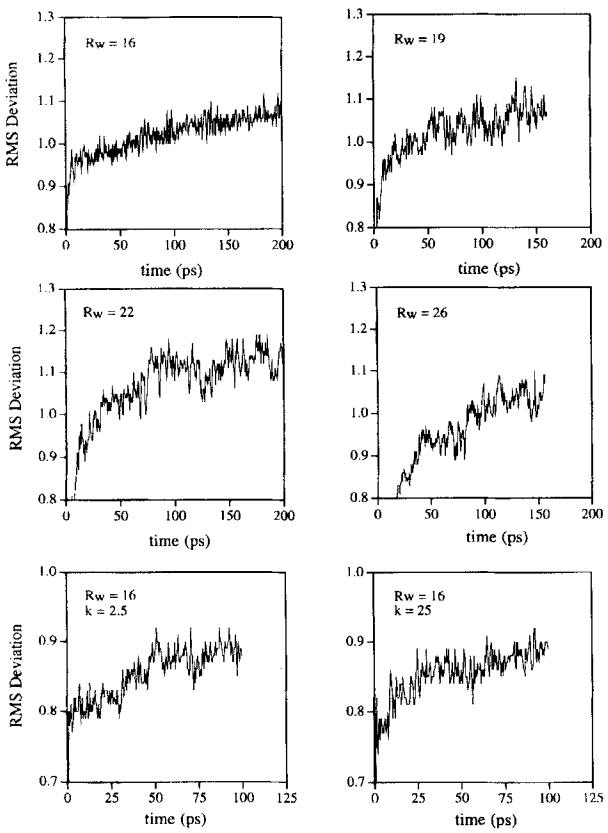

FIGURE 3. The rms deviations (Å) from the X-ray coodinates of the DHFR molecule as a function of simulation time for the tethered water (TW) model. R_w is the radius (Å) of the solvation sphere. The force constant for the restraining potential is k = 0.005 kcal/ mol/ Å^2, unless specified for k = 25 and k = 2.5 kcal/ mol/ Å^2.

TW (R_w = 22 Å) model. The only waters conserved in Figures 6 and 7 are numbers 244 (crystallographic) and 586 (added solvent), both of which interact strongly with the ligand–protein salt-bridge. Crystallographic water molecules 244 and 281 both appear in Figures 7 and 8. Except for crystallographic water 244, which is buried deeper within the binding pocket and conserved in all structures, the active-site water molecules appear to be highly mobile, and would readily exchange with the bulk solvent.

FREE ENERGY CHANGES

It is known from our previous studies on 8-substituted pterins and N5-deazapterins that the contributions to the free energies due to mutation of vdW terms is quite small and these contributions cancel when differences are taken.[20,21,28] Consequently, in Table VII we report the free-energy

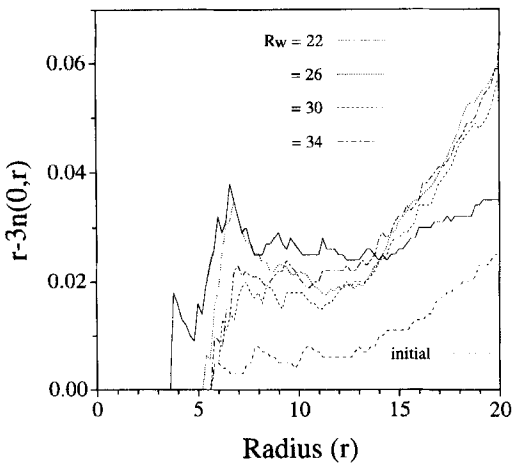

FIGURE 4. Solvent densities (Å^{-3}) as a function of distance (Å) from the C8a atom of the 8-methyl-N5-deazapterin ligand for the capped water (CW) model. The "initial" distribution is for the bulk-solvent density. R_w is the radius (Å) of the solvation sphere. $n(0, r)$ is the number of solvent molecules within radius r. Averages obtained over 4 ps of trajectories by sampling configurations at 0.1-ps intervals.

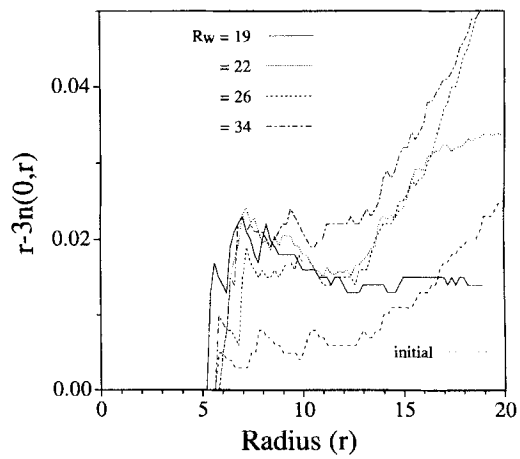

FIGURE 5. Solvent densities (Å^{-3}) as a function of distance (Å) from the C8a atom of the 8-methyl-N5-deazapterin ligand comparing the tethered water (TW; R_w = 19, 22, and 26 Å, k = 0.005 kcal/ mol/ Å^2) models and the capped water (CW; R_w = 34 Å) model (CW model shown in Fig. 7 also). The "initial" distribution is for the bulk-solvent density. R_w is the radius (Å) of the solvation sphere. $n(0, r)$ is the number of solvent molecules within radius r. Averages obtained over 4 ps of trajectories by sampling configurations at 0.1-ps intervals.

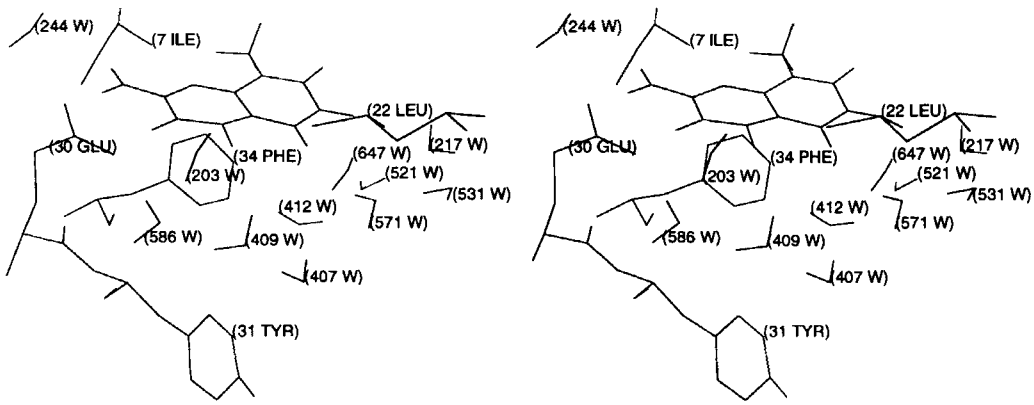

FIGURE 6. Stereoview of the active site of DHFR taken from the final configuration in the MD trajectory for the CW (R_w = 22 Å) model.

change for mutation of electrostatic terms only, with a 9-Å cutoff, and no cutoff for ligand–protein and ligand–solvent interactions. As may be seen from Table VII, a range of binding free energies spanning ~ 2 kcal/mol is obtained. Previous calculations were performed with a cutoff of 8 Å for the nonbonded interactions.[21] However, it is clear from the present calculations that substantial errors (ca. 1.5 kcal/mol) may result from truncation of the long-range electrostatic forces. Consequently, in the following discussion we give a revised estimate of the relative affinities for DHFR.

With no cutoff for the nonbonded interactions between ligand and the rest of the system, the TW (R_w = 22 Å) model gives the smallest free energy change of -2.56 ± 0.04 kcal/mol, whereas the largest change (-4.01 ± 0.08 kcal/mol) is obtained for the unsolvated CW (R_w = 16 Å) model. The solvated models give absolute values of free energies about 1 kcal/mol below those obtained from the unsolvated (R_w = 16 Å) models. However, the variation of the free energy with the type of solvent model is much less than 1 kcal/mol. The difference between CW and TW models is ca. 0.4 kcal/mol, whereas the difference between R_w = 22 and R_w = 26 Å for both models is only ca. 0.1 kcal/mol. These results suggest that, while the free energies are clearly affected by the presence of explicit solvent, the fine details of the solvent distribution and protein structural changes are of lesser importance. This conclusion also tends to be supported by comparing the results obtained for the tethering potentials k = 2.5 and k = 0.005. Although the results for k = 0.005 (R_w = 16 Å) deviate more from the initial X-ray structure as measured by overall rms deviations (Table III), the difference in the computed free energy is less than 0.2 kcal/mol. Note, however, that significantly larger free energy differences between solvent–protein structures are obtained with the 9-Å cutoff. The apparent insensitivity with respect to the solvent model obtained with no cutoff is therefore due to an averaging effect of the long-range electrostatic interactions.

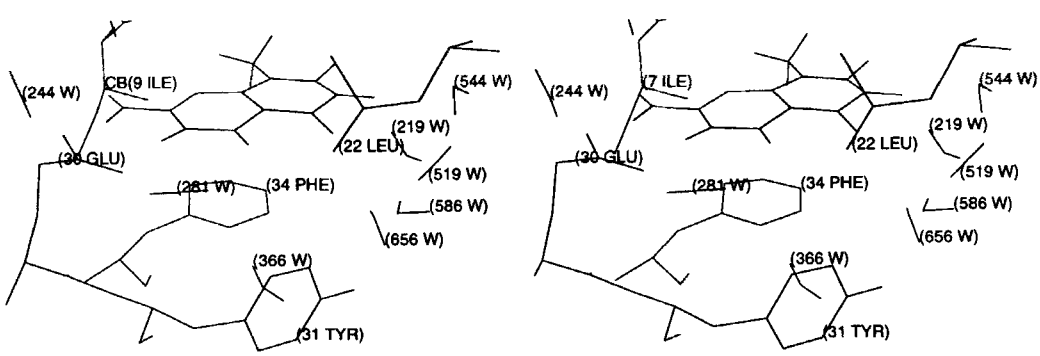

FIGURE 7. Stereoview of the active site of DHFR taken from the final configuration in the MD trajectory for the TW (R_w = 22 Å) model.

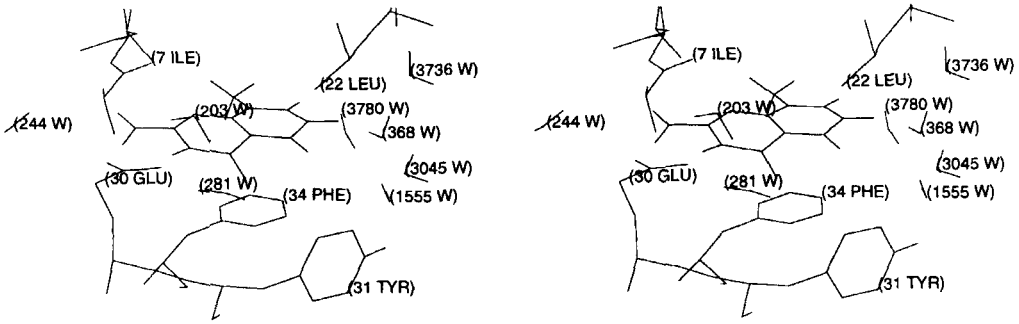

FIGURE 8. Stereoview of the active site of DHFR taken from the final configuration in the MD trajectory for the CW (R_w = 34 Å) model.

The relative thermodynamic stability of the binding is given by the difference in ΔA [eq. (11)] for ligand bound to DHFR (ΔA_{bind}) and free ligand in solution (ΔA_{solv}). This latter solvation free energy has been calculated previously to be in the range 3.7 to 4.2 kcal/mol, using parameter sets derived from the AM1 model for the ligands.[28] Assuming a value of −4.0 kcal/mol for ΔA_{solv},[28] a value of −2.7 kcal/mol (TW model, R_w = 26 Å, k = 0.005) for ΔA_{bind} gives a difference ($\Delta A_{bind} - \Delta A_{solv}$) in binding free energy of 1.3 kcal/mol, which may be compared with the experimental value of ±0.2 kcal/mol.[16-18]

TABLE VII.
Free Energies (kcal / mol) Calculated Using Solvated-Protein Models.

Model[a]	R_w[b]	N_w[c]	ΔA_{bind}[d] 9 Å[e]	No cutoff[e]
CW	16	46	−4.88 ± 0.02	−3.74 ± 0.13
CW	22	392	−3.83 ± 0.04	−2.98 ± 0.25
CW	26	1033	−4.19 ± 0.03	−3.04 ± 0.07
TW (k = 2.5)	16	46	−4.22 ± 0.19	−4.01 ± 0.08
TW (k = 0.005)	16	46	−4.78 ± 0.01	−3.85 ± 0.18
TW (k = 0.005)	22	392	−4.23 ± 0.30	−2.56 ± 0.04
TW (k = 0.005)	26	1033	−3.43 ± 0.12	−2.67 ± 0.23

[a] CW = capped water, TW = tethered water (see text). k = force constant for restraining potential (kcal/ mol/ Å^2).
[b] Radius (Å) of solvation sphere.
[c] Numbers of dynamical water molecules within solvation sphere.
[d] Mean and standard error for the forward (i.e., 8-methyl-N5-deazapterin → 8-methylpterin) and reverse mutation of the electrostatic force-field.
[e] Cutoff for protein–ligand and solvent–ligand interaction; all other interactions are subject to a 9-Å cutoff.

Conclusion

Although it is usually not feasible to include the bulk of the solvent explicitly in macromolecular dynamics simulations, relatively large numbers of explicit surface water molecules are required to describe adequately the effect of specific H-bonding interactions and the solvation of binding pockets. However, the simple inclusion of a solvent layer is inadequate as neglect of the bulk is known to be critical to solvent behavior near the protein surface. In the present work on DHFR, the effect of this bulk on the dynamics of surface water has been modeled by the introduction of harmonic restraining potentials. We found that smaller shells of dynamically restrained water molecules yielded active sites that are similar to those obtained using much larger solvent shells of unrestrained molecules, without the artifacts and distortions that were apparent when restraining potentials were not used. This trend suggests that shells of restrained water would be an efficient model for bulk solvent in both active-site MD simulations and unconstrained-protein dynamics.[22] Moreover, we found that the value of 0.005 kcal/mol/Å^2 for the restraint used by Solmajer and Mehler in BPTI simulations[22] works quite well for the active site of DHFR also. This value gave satisfactory results over a range of solvent shell sizes, and an order of magnitude estimate of 10^{-2} to 10^{-3} kcal/mol/Å^2 may well be suitable for most protein–solvent systems. Larger values of the force constant resulted in protein structures that are too similar to the initial X-ray structure. However, whereas use of the distance-dependent dielectric function in conjunction with a limited number of restrained water molecules is recommended by Solmajer and Mehler,[22] our experience is that the use of dielec-

tric functions causes distorting effects in an active-site dynamics approach and they are thus unsuitable. Also, dielectric functions are clearly not well suited to free energy simulations as the scaling of interaction energies would lead to an underestimation of the free-energy change, which would then need to be corrected. The effect of ignoring solvent is likely to introduce errors comparable with those due to truncation of electrostatic interactions, i.e., of the order of 1–2 kcal/mol. However, the present results indicate that the free energies are not very sensitive to the model used to describe bulk solvent effects provided sufficient numbers of waters are included in the simulation.

Acknowledgments

This work was financed by grants from the National Health and Medical Research Council (NH & MRC), and equipment grants from the Clive and Vera Ramaciotti and Utah Foundations. We are most grateful to Australian Supercomputer Technology for generous allocations of time on their FACOM 2200 supercomputer.

References

1. T. Solmajer and E. L. Mehler, *Prot. Eng.*, **4**, 911 (1991).
2. G. E. Arnold and R. L. Ornstein, *Proteins*, **18**, 19 (1994).
3. K. A. Sharp, In *Computer Simulation of Biomolecular Systems*, Vol. 2, W. F. van Gunsteren, P. K. Weiner, and A. J. Wilkinson, Eds., ESCOM, Leiden, 1993, pp. 147–160.
4. B. von Freyberg and W. Braun, *J. Comput. Chem.*, **5**, 510 (1993).
5. F. Floris and J. Tomasi, *J. Comput. Chem.*, **10**, 616 (1989).
6. W. F. van Gunsteren and H. J. C. Berendsen, *J. Mol. Biol.*, **176**, 559 (1984).
7. C. F. Wong and J. A. McCammon, *Israel J. Chem.*, **27**, 211 (1986).
8. P. Ahlström, O. Teleman, and B. Jönsson, *J. Am. Chem. Soc.*, **110**, 4198 (1988).
9. Y. Komeiji, M. Uebayasi, J. Someya, and I. Yamato, *Proteins*, **16**, 268 (1993).
10. D. S. Harlsough and K. M. Merz, *J. Am. Chem. Soc.*, **115**, 6529 (1993).
11. M. Berkowitz and J. A. McCammon, *Chem. Phys. Lett.*, **90**, 215 (1982).
12. C. L. Brooks, A. Brunger, and M. Karplus, *Biopolymers*, **24**, 843 (1985).
13. M. Mezei and D. L. Beveridge, *Ann. NY Acad. Sci.*, **482**, 1 (1986).
14. C. A. Reynolds, P. M. King, and W. G. Richards, *Mol. Phys.*, **76**, 251 (1992).
15. R. L. Blakley, In *Folates and Pterins, Chemistry and Biochemistry of Folates*, Vol. 1. R. L. Blakley and S. J. Benkovic, Eds., Wiley, New York, 1984, pp. 191–253.
16. V. Thibault, M. J. Koen, and J. E. Gready, *Biochemistry*, **24**, 4761 (1985).
17. M. T. G. Ivery and J. E. Gready, *Biochemistry*, **34**, 3724 (1995).
18. M. T. G. Ivery and J. E. Gready, *J. Med. Chem.*, **37**, 4211 (1994).
19. J. E. Gready, In *Chemistry and Biology of Pteridines 1989*, H.-Ch Curtius, S. Ghisla, and N. Blau, Eds., de Gruyter, Berlin, 1990, pp. 23–30.
20. P. L. Cummins and J. E. Gready, *Proteins Struct. Funct. Genet.*, **15**, 426 (1993).
21. P. L. Cummins and J. E. Gready, *J. Comput.-Aided Mol. Design*, **7**, 535 (1993).
22. T. Solmajer and E. L. Mehler, *Int. J. Quant. Chem.*, **44**, 291 (1992).
23. K. S. Kim, *Chem. Phys. Lett.*, **156**, 261 (1989).
24. S. J. Weiner, P. A. Kollman, D. T. Nguyen, and D. A. Case, *J. Comput. Chem.*, **7**, 230 (1986).
25. S. J. Weiner, P. A. Kollman, D. A. Case, U. C. Singh, C. Ghio, G. Alagona, S. Profeta, and P. Weiner, *J. Am. Chem. Soc.*, **106**, 765 (1984).
26. P. L. Cummins, K. Ramnarayan, U. C. Singh, and J. E. Gready, *J. Am. Chem. Soc.*, **113**, 8247 (1991).
27. M. J. S. Dewar, E. G. Zoebisch, E. F. Healy, and J. J. P. Stewart, *J. Am. Chem. Soc.*, **107**, 3902 (1985).
28. P. L. Cummins and J. E. Gready, *J. Comput. Chem.*, **15**, 704 (1994).
29. W. L. Jorgensen, J. Chandrasekhar, J. D. Madura, R. W. Impey, and M. L. Klein, *J. Chem. Phys.*, **79**, 926 (1983).
30. A. T. Hagler, S. Lifson, and P. Dauber, *J. Am. Chem. Soc.*, **101**, 5122 (1979).
31. A. T. Hagler, J. R. Maple, T. S. Thacher, G. B. Fitzgerald, and U. Dinur, In *Computer Simulation of Biomolecular Systems*, W. F. van Gunsteren and P. K. Weiner, Eds., ESCOM, Leiden, 1989, pp. 149–167.
32. S. Hirono and P. A. Kollman, *J. Mol. Biol.*, **212**, 196 (1990).
33. M. A. McTigue, J. F. Davies, B. T. Kaufman, and J. Kraut, *Biochemistry*, **31**, 7264 (1992).
34. H. J. C. Berendsen, J. P. M. Postma, W. F. van Gunsteren, A. DiNola, and J. R. Haak, *J. Chem. Phys.*, **81**, 3684 (1984).
35. W. F. van Gunsteren and H. J. C. Berendsen, *Mol. Phys.*, **34**, 1311 (1977).
36. J. J. Wendoloski and J. B. Matthews, *Proteins Struct. Funct. Genet.*, **5**, 313 (1989).
37. J. Geunot and P. A. Kollman, *Protein Sci.*, **1**, 1185 (1992).
38. P. E. Smith and W. F. van Gunsteren, In *Computer Simulation of Biomolecular Systems*, Vol. 2, W. F. van Gunsteren, P. K. Weiner, and A. J. Wilkinson, Eds., ESCOM, Leiden, 1993, pp. 182–212.